Joint inversion of PP- and PSV-wave amplitude data for estimating P- and S-wave moduli and attenuation factor

Huaizhen Chen*, Shahpoor Moradi and Kristopher A. Innanen

ABSTRACT

Beginning with re-expressing P- and S-wave velocities in anelastic media, we first propose frequency-dependent P- and S-wave moduli in terms of P- and S-wave moduli at a reference frequency and P-wave maximum attenuation factor, in which we replace S-wave attenuation factor with P-wave maximum attenuation factor. Based on Zoeppritz equations and their linearized expressions for computing PP and PSV-wave reflection coefficients, we derive frequency-component PP- and PSV-wave reflection coefficients as a function of P-wave maximum attenuation factor, from which anelastic impedances for PP- and PSV waves are expressed. Using the derived reflection coefficients and elastic impedances, we establish a two-step inversion approach, which involves the estimation of attenuative PP- and PSV-wave anelastic impedances from frequency-components of partially-stacked seismic data, and the prediction of unknown parameter vector (P- and S-wave moduli, density and P-wave maximum attenuation factor) using the estimated PP- and PSV-wave anelastic impedances. Synthetic tests confirm that the unknown parameters are estimated stably and reliably in the case of seismic data containing a moderate Gaussian noise. Applying the inversion approach to a real data set acquired over an oil-bearing reservoir, we observe reasonable results of P-wave maximum attenuation factor are obtained, which may provide additional proofs for fluid identification.

INTRODUCTION

Attenuation factor $1/Q$ is sensitive to rock properties (shale volume, porosity and permeability) and fluid content, which is useful for reservoir characterization. In the case of fractured rocks, seismic wave propagation is strongly affected by fractures and fluids within fractures. For the partially liquid-saturated fractured rock (e.g. fractures are filled with the mixture of gas and oil), seismic wave amplitude is influenced by frequency-dependent attenuation (Berryman, 2007). Based on attenuation rock physics theory and effective models, geophysicists can analyze how the attenuation factor changes with rock properties and fluids given different values of frequency and implement the estimation of attenuation using seismic amplitude data.

Many rock physics effective models are proposed for describing how wave propagates in saturated or partially-saturated porous media. Biot (1956a,b) presents theory of propagation of elastic waves in fluid-saturated rocks in low- and high-frequency ranges, and he also discusses how to compute frequency-dependent velocities of saturated rocks. To solve the problem of fluid substitution, Gassmann (1951) propose an effective model to calculate saturated-rock moduli from dry-rock moduli, which works best in seismic frequency range under the condition of isotropic rocks; Gassmann (1951) and Brown and Korringa (1975) respectively discuss how to compute stiffness and compliance parameters of anisotropic rocks. In the case of a rock containing both compliant and stiff pores, fluid movement appears when seismic wave compresses the rock. The squirt model is proposed by Mavko

and Jizba (1991), which is used for predicting high-frequency moduli of saturated rocks. Dvorkin et al. (1995) extend the squirt model to compute the moduli of saturated rocks at any frequency, which means the extended squirt model can be effectively employed to calculate elastic properties and attenuation factors of saturated rocks in seismic frequency range. In the case of partially-saturated rocks, the Biot–squirt (BISQ) model is proposed by Dvorkin and Nur (1993) and Dvorkin et al. (1994) to compute elastic moduli and attenuation factors of rocks. Dvorkin and Mavko (2006) present a set of equations to utilize low- and high-frequency limits of elastic moduli to compute frequency-dependent P- and S-wave inverse quality factors for partially- and fully-saturated rocks.

The effect of attenuation factor on reflection coefficient has been studied. Morozov (2011) studies anelastic acoustic impedance in detail and explains how attenuation constrasts produce phase-shifted reflections. Based on extended Zoeppritz equations, Innanen (2011) presents expressions of attenuative reflection coefficients of P and S waves in terms of perturbations in P- and S-wave quality factors Q_{P} and Q_{S}. Using the reflection coefficients amplitude-variation-with-frequency (AVF) data are employed to estimate attenuation factors $1/Q_{\mathrm{P}}$ and $1/Q_{\mathrm{S}}$ (Innanen, 2011; Bird, 2012). Moradi and Innanen (2015, 2016) propose expressions of scattering of homogeneous and inhomogeneous seismic waves in low-loss viscoelastic media and express how reflection coefficients vary with offset and how features of amplitude variation with offset/angle (AVO/AVA) are influenced by attenuation angle. Starting with attenuative rock physics model, Chen et al. (2018) propose frequency-dependent reflection coefficient and anelastic impedance as a function of P- and S-wave attenuation factors. Based on the derived reflection coefficient and anelastic impedance, Chen et al. (2018) implement a nonlinear inversion of seismic data for estimating attenuation factors.

In the present study, we begin with re-expressing P- and S-wave velocities and moduli in terms of P-wave attenuation factor, in which a relationship between P- and S-wave attenuation factors is employed. Based on the re-expressed P- and S-wave moduli, we derive approximate and linearized frequency-dependent PP- and PSV-wave reflection coefficients by solving the Zoeppritz equations, and we also present expression of anelastic impedances of PP and PSV waves using the derived reflection coefficients. We present a two-step inversion approach of employing partially-incidence-stacked PP- and PSV-wave seismic data to estimate the unknown parameter vector involving P- and S-wave moduli, density and P-wave attenuation factor, which is implemented as: the estimation of PP- and PSV-wave anelastic impedances using frequency components of partially-incidence-stacked seismic data; the prediction of the unknown parameter vector by computing a full Newton step using the estimated anelastic impedances results. Synthetic tests confirm the proposed inversion approach is stable and robust. Real data case verifies that reliable results of P- and S-wave moduli and P-wave attenuation factor can be estimated, which may provide an additional proof for reservoir characterization and fluid identification.

THEORY AND METHOD

In this section, we will first clarify how to rewrite P- and S-wave velocities as a function of P-wave maximum inverse quality factor based on an expression of elastic wave velocity proposed by Aki and Richards (2002); then we will derive frequency-dependent PP-

and PSV-wave linearized reflection coefficients in terms of P- and S-wave moduli, density and P-wave maximum inverse quality factor, from which corresponding PP- and PSV-wave elastic impedances and their normalized versions will be generated; and finally we will establish a two-step inversion approach, which involves inversion of partially-stacked seismic data for elastic impedances, and estimation of unknown parameters (i.e. P- and S-wave moduli, density, and P-wave maximum attenuation factor) from the inversion results of elastic impedances.

Expressions of P- and S-wave velocities in attenuating media

In attenuating media, the complex elastic wave velocity $\widetilde{V}$ expressed as a function of frequency-dependent phase velocity $V(\omega)$ and attenuation factor $\frac{1}{Q(\omega)}$ is given by Aki and Richards (2002)

$$\widetilde{V} = V(\omega)\left[1 - \frac{i}{2Q(\omega)}\right], \tag{1}$$

where $\omega = 2\pi f$, and f is frequency.

Given a reference frequency ω_r, the complex wave velocity is expressed as (Aki and Richards, 2002)

$$\widetilde{V} = V(\omega_r)\left[1 + \frac{1}{\pi Q(\omega)}\log\left(\frac{\omega}{\omega_r}\right) - \frac{i}{2Q(\omega)}\right], \tag{2}$$

where $V(\omega_r)$ is the velocity at the reference frequency ω_r. We next replace the frequency-dependent attenuation factor $1/Q(\omega)$ with a constant attenuation factor. Following Dvorkin and Mavko (2006), we rewrite the frequency-dependent attenuation factor as

$$\frac{1}{Q(\omega)} = \frac{1}{Q_{\mathrm{m}}}\eta(\omega), \tag{3}$$

where $\frac{1}{Q_{\mathrm{m}}}$ is the maximum of attenuation factor, $\eta(\omega) = \frac{2\omega/\omega_c}{1+(\omega/\omega_c)^2}$, and ω_c is the critical frequency at which the attenuation factor reaches its maximum. For P-wave propagation in attenuating media, the attenuation factor is given by

$$\frac{1}{Q_{\mathrm{P}}(\omega)} = \frac{1}{Q_{\mathrm{Pm}}}\eta(\omega), \tag{4}$$

where $\frac{1}{Q_{\mathrm{Pm}}}$ is the maximum of P-wave attenuation factor. Mavko et al. (2009) proposed a relationship between P-wave attenuation factor and S-wave attenuation factor, and in the present study, the relationship is extended to be frequency-dependent

$$\frac{1/[Q_{\mathrm{P}}(\omega)]}{1/[Q_{\mathrm{S}}(\omega)]} = \frac{1}{4}\frac{[1-2g(\omega)]^2[3-2g(\omega)]}{g(\omega)[1-g(\omega)]} = h(\omega), \tag{5}$$

where $\frac{1}{Q_{\mathrm{S}}(\omega)}$ is frequency-dependent S-wave attenuation factor, and $g(\omega)$ is attenuating S-to-P wave moduli ratio. Combining equations (4) and (5), we re-express the S-wave attenuation factor as

$$\frac{1}{Q_{\mathrm{S}}(\omega)} = \frac{1}{Q_{\mathrm{Pm}}}\frac{\eta(\omega)}{h(\omega)}. \tag{6}$$

Combining equations (2) and (4), we obtain the complex P-wave velocity $\widetilde{V_{\mathrm{P}}}$ in attenuating media

$$\begin{aligned}\widetilde{V_{\mathrm{P}}} &= V_{\mathrm{P}}(\omega_r)\left[1+\frac{1}{\pi Q_{\mathrm{P}}(\omega)}\log\left(\frac{\omega}{\omega_r}\right)-\frac{i}{2Q_{\mathrm{P}}(\omega)}\right]\\ &= \alpha\left[1+\frac{1}{\pi Q_{\mathrm{Pm}}}\psi(\omega)-\frac{i}{2Q_{\mathrm{Pm}}}\eta(\omega)\right],\end{aligned} \tag{7}$$

where $\psi(\omega)=\log\left(\frac{\omega}{\omega_c}\right)\eta(\omega)$, and $\alpha = V_{\mathrm{P}}(\omega_c)$. It is important to stress that we use the critical frequency as the reference frequency in equation (2) (i.e. $\omega_r = \omega_c$). For S-wave, the complex velocity $\widetilde{V_{\mathrm{S}}}$ is given by

$$\begin{aligned}\widetilde{V_{\mathrm{S}}} &= V_{\mathrm{S}}(\omega_r)\left[1+\frac{1}{\pi Q_{\mathrm{S}}(\omega)}\log\left(\frac{\omega}{\omega_r}\right)-\frac{i}{2Q_{\mathrm{S}}(\omega)}\right]\\ &= \beta\left[1+\frac{1}{\pi Q_{\mathrm{Pm}}}\frac{\psi(\omega)}{h(\omega)}-\frac{i}{2Q_{\mathrm{Pm}}}\frac{\eta(\omega)}{h(\omega)}\right],\end{aligned} \tag{8}$$

where $\beta = V_{\mathrm{S}}(\omega_c)$. Following Chen et al. (2018), we assume the characteristic frequency falls into well log frequency range, and in this study, we let the characteristic frequency be $10000\mathrm{Hz}$.

We next compare real and imaginary parts of P- and S-wave velocities in the case of different values of P-wave maximum attenuation factor and frequency, as plotted in Figure 1. We observe that the imaginary parts of P- and S-wave velocities are much smaller than the corresponding real parts in the case that the attenuation factor is not too small (e.g. $1/Q_{\mathrm{Pm}} \geq 0.1$). It indicates that the imaginary part is negligible in attenuating media; hence the new expressions of P- and S-wave velocities are given by

$$\begin{aligned}\mathcal{V}_{\mathrm{P}} &= \alpha\left[1+\frac{1}{\pi Q_{\mathrm{Pm}}}\psi(\omega)\right],\\ \mathcal{V}_{\mathrm{S}} &= \beta\left[1+\frac{1}{\pi Q_{\mathrm{Pm}}}\frac{\psi(\omega)}{h(\omega)}\right].\end{aligned} \tag{9}$$

Assuming a density that is independent of frequency, we express P- and S-wave moduli ($\mathcal{M}$ and $\mathcal{U}$) as

$$\begin{aligned}\mathcal{M} &\approx M\left[1+\frac{2}{\pi Q_{\mathrm{Pm}}}\psi(\omega)\right],\\ \mathcal{U} &\approx \mu\left[1+\frac{2}{\pi Q_{\mathrm{Pm}}}\frac{\psi(\omega)}{h(\omega)}\right],\end{aligned} \tag{10}$$

where $M = \rho\alpha^2$, $\mu = \rho\beta^2$, and we neglect the term proportional to $\frac{1}{(Q_{\mathrm{Pm}})^2}$ under the assumption that $Q_{\mathrm{Pm}} \ll 1$.

Derivation of linearized reflection coefficients for PP and PSV-waves in attenuating media

Ikelle and Amundsen (2005) present expressions of PP- and PSV-wave reflection coef-

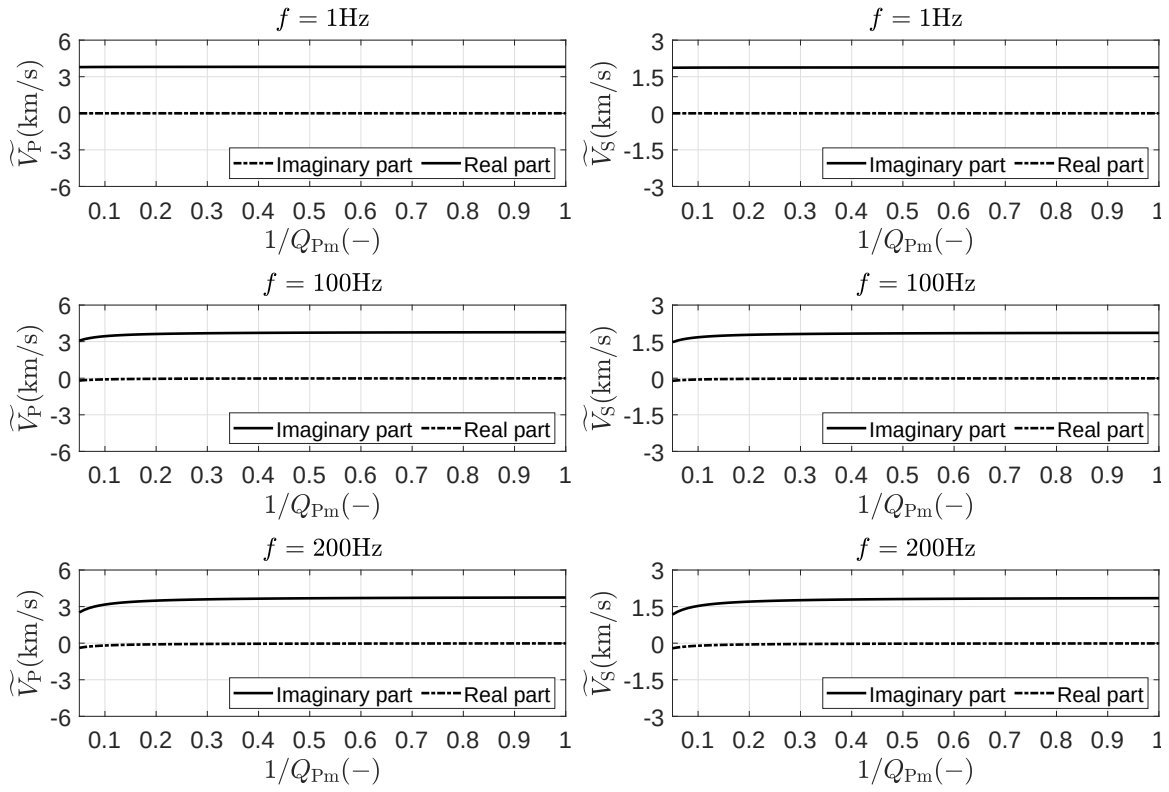

FIG. 1. Comparisons between real and imaginary parts of P- and S-wave velocities. Quantities $\alpha = 3.81$km/s, and $\beta = 1.88$km/s.

ficients ($R_{\rm PP}$ and $R_{\rm PS}$) by solving the Zoeppritz equations

$$\begin{aligned} R_{\rm PP} &= \frac{\Gamma_1\Omega_2 - \Gamma_3\Omega_4}{\Omega_1\Omega_2 + \Omega_4\Omega_3}, \\ R_{\rm PS} &= -\left(\frac{\mathcal{V}_{\rm P1}}{\mathcal{V}_{\rm S1}}\right)\frac{\Gamma_3\Omega_1 + \Gamma_1\Omega_3}{\Omega_1\Omega_2 + \Omega_4\Omega_3}, \end{aligned} \tag{11}$$

where

$$\begin{aligned} &\Omega_1 = -2k^2\Delta\mathcal{U}\left(q_{\rm P1} - q_{\rm P2}\right) + \left(\rho_1 q_{\rm P2} + \rho_2 q_{\rm P1}\right), \Omega_2 = -2k^2\Delta\mathcal{U}\left(q_{\rm S1} - q_{\rm S2}\right) + \left(\rho_1 q_{\rm S2} + \rho_2 q_{\rm S1}\right), \\ &\Omega_3 = -k\left[2\Delta\mathcal{U}\left(q_{\rm P1}q_{\rm S2} + k^2\right) - \Delta\rho\right], \Omega_4 = -k\left[2\Delta\mathcal{U}\left(q_{\rm P2}q_{\rm S1} + k^2\right) - \Delta\rho\right], \\ &\Gamma_1 = -2k^2\Delta\mathcal{U}\left(q_{\rm P1} + q_{\rm P2}\right) - \left(\rho_1 q_{\rm P2} - \rho_2 q_{\rm P1}\right), \Gamma_3 = k\left[2\Delta\mathcal{U}\left(q_{\rm P1}q_{\rm S2} - k^2\right) + \Delta\rho\right], \\ &q_{\rm P1} = \sqrt{\mathcal{V}_{\rm P1}^{-2} - k^2}, q_{\rm S1} = \sqrt{\mathcal{V}_{\rm S1}^{-2} - k^2}, \\ &q_{\rm P2} = \sqrt{\mathcal{V}_{\rm P2}^{-2} - k^2}, q_{\rm S2} = \sqrt{\mathcal{V}_{\rm S2}^{-2} - k^2}, \end{aligned} \tag{12}$$

in which $\Delta\mathcal{U}$ and $\Delta\rho$ are differences in S-wave modulus and density between top and bottom layers across the interface, $\mathcal{V}_{\rm P1}$ and $\mathcal{V}_{\rm P2}$ are frequency-dependent P-wave velocities of top and bottom layers respectively, $\mathcal{V}_{\rm S1}$ and $\mathcal{V}_{\rm S2}$ are frequency-dependent S-wave velocities of top and bottom layers respectively, and k is ray parameter given by

$$k = \frac{\sin\theta_{\rm P1}}{\mathcal{V}_{\rm P1}} = \frac{\sin\theta_{\rm P2}}{\mathcal{V}_{\rm P2}} = \frac{\sin\theta_{\rm S1}}{\mathcal{V}_{\rm S1}} = \frac{\sin\theta_{\rm S2}}{\mathcal{V}_{\rm S2}}, \tag{13}$$

where θ_{P1} and θ_{S1} are P- and S-wave incidence angles in the top layer, and θ_{P2} and θ_{S2} are P- and S-wave transmission angles in the bottom layer, respectively.

Following Moradi and Innanen (2016), we rewrite frequency-dependent P- and S-wave velocities, P- and S-wave incidence and transmission angles, and density of top and bottom layers as

$$\begin{aligned}
&\rho_1 = \rho\left(1-\frac{1}{2}\frac{\Delta\rho}{\rho}\right), \rho_2 = \rho\left(1+\frac{1}{2}\frac{\Delta\rho}{\rho}\right),\\
&\mathcal{V}_{\mathrm{P1}} = \mathcal{V}_{\mathrm{P}}\left(1-\frac{1}{2}\frac{\Delta\mathcal{V}_{\mathrm{P}}}{\mathcal{V}_{\mathrm{P}}}\right), \mathcal{V}_{\mathrm{P2}} = \mathcal{V}_{\mathrm{P}}\left(1+\frac{1}{2}\frac{\Delta\mathcal{V}_{\mathrm{P}}}{\mathcal{V}_{\mathrm{P}}}\right),\\
&\mathcal{V}_{\mathrm{S1}} = \mathcal{V}_{\mathrm{S}}\left(1-\frac{1}{2}\frac{\Delta\mathcal{V}_{\mathrm{S}}}{\mathcal{V}_{\mathrm{S}}}\right), \mathcal{V}_{\mathrm{S2}} = \mathcal{V}_{\mathrm{S}}\left(1+\frac{1}{2}\frac{\Delta\mathcal{V}_{\mathrm{S}}}{\mathcal{V}_{\mathrm{S}}}\right),\\
&\sin\theta_{\mathrm{P1}} = \sin\theta_{\mathrm{P}}\left(1-\frac{1}{2}\frac{\Delta\theta_{\mathrm{P}}}{\tan\theta_{\mathrm{P}}}\right), \sin\theta_{\mathrm{P2}} = \sin\theta_{\mathrm{P}}\left(1+\frac{1}{2}\frac{\Delta\theta_{\mathrm{P}}}{\tan\theta_{\mathrm{P}}}\right),\\
&\sin\theta_{\mathrm{S1}} = \sin\theta_{\mathrm{S}}\left(1-\frac{1}{2}\frac{\Delta\theta_{\mathrm{S}}}{\tan\theta_{\mathrm{S}}}\right), \sin\theta_{\mathrm{S2}} = \sin\theta_{\mathrm{S}}\left(1+\frac{1}{2}\frac{\Delta\theta_{\mathrm{S}}}{\tan\theta_{\mathrm{S}}}\right).
\end{aligned} \tag{14}$$

Combining equations (12) and (13), we express perturbation in incidence angles as

$$\begin{aligned}
\Delta\theta_{\mathrm{P}} &\approx \frac{\Delta\mathcal{V}_{\mathrm{P}}}{\mathcal{V}_{\mathrm{P}}}\tan\theta_{\mathrm{P}},\\
\Delta\theta_{\mathrm{S}} &\approx \frac{\Delta\mathcal{V}_{\mathrm{S}}}{\mathcal{V}_{\mathrm{S}}}\tan\theta_{\mathrm{S}}.
\end{aligned} \tag{15}$$

Combining equations (11)-(15), we obtain the PP- and PSV-wave reflection coefficients as

$$\begin{aligned}
R_{\mathrm{PP}} &\approx \frac{1}{4\cos^2\theta_{\mathrm{P}}}\frac{\Delta\mathcal{M}}{\mathcal{M}} - 2g(\omega)\sin^2\theta_{\mathrm{P}}\frac{\Delta\mathcal{U}}{\mathcal{U}} + \frac{\cos 2\theta_{\mathrm{P}}}{4\cos^2\theta_{\mathrm{P}}}\frac{\Delta\rho}{\rho},\\
R_{\mathrm{PS}} &\approx \sqrt{g(\omega)}\sin\theta_{\mathrm{P}}\left(\frac{\sqrt{g(\omega)}\sin^2\theta_{\mathrm{P}}}{\sqrt{1-g(\omega)\sin^2\theta_{\mathrm{P}}}} - \cos\theta_{\mathrm{P}}\right)\frac{\Delta\mathcal{U}}{\mathcal{U}} - \frac{g(\omega)\sin\theta_{\mathrm{P}}}{2\sqrt{1-g(\omega)\sin^2\theta_{\mathrm{P}}}}\frac{\Delta\rho}{\rho},
\end{aligned} \tag{16}$$

where $g(\omega) = \frac{\mathcal{U}}{\mathcal{M}}$. Using equation (10) we may approximately express $\frac{\Delta\mathcal{M}}{\mathcal{M}}$ and $\frac{\Delta\mathcal{U}}{\mathcal{U}}$ as

$$\begin{aligned}
\frac{\Delta\mathcal{M}}{\mathcal{M}} &= \frac{\Delta\left\{M\left[1+\frac{2}{\pi Q_{\mathrm{Pm}}}\psi(\omega)\right]\right\}}{M\left[1+\frac{2}{\pi Q_{\mathrm{Pm}}}\psi(\omega)\right]} \approx \frac{\Delta M}{M} + \frac{2\psi(\omega)}{\pi}\Delta\left(\frac{1}{Q_{\mathrm{Pm}}}\right),\\
\frac{\Delta\mathcal{U}}{\mathcal{U}} &= \frac{\Delta\left\{\mu\left[1+\frac{2}{\pi Q_{\mathrm{Pm}}}\frac{\psi(\omega)}{h(\omega)}\right]\right\}}{\mu\left[1+\frac{2}{\pi Q_{\mathrm{Pm}}}\frac{\psi(\omega)}{h(\omega)}\right]} \approx \frac{\Delta\mu}{\mu} + \frac{2}{\pi}\frac{\psi(\omega)}{h(\omega)}\Delta\left(\frac{1}{Q_{\mathrm{Pm}}}\right).
\end{aligned} \tag{17}$$

Substituting equation (17) into equation (16) we obtain final expressions of frequency-dependent PP- and PSV-wave reflection coefficients

$$\begin{aligned}
R_{\mathrm{PP}}(\theta_{\mathrm{P}},\omega) &\approx a_M(\theta_{\mathrm{P}})\frac{\Delta M}{M} + a_\mu(\theta_{\mathrm{P}})\frac{\Delta\mu}{\mu} + a_\rho(\theta_{\mathrm{P}})\frac{\Delta\rho}{\rho} + a_Q(\theta_{\mathrm{P}},\omega)\Delta\left(\frac{1}{Q_{\mathrm{Pm}}}\right),\\
R_{\mathrm{PS}}(\theta_{\mathrm{P}},\omega) &\approx b_\mu(\theta_{\mathrm{P}})\frac{\Delta\mu}{\mu} + b_\rho(\theta_{\mathrm{P}})\frac{\Delta\rho}{\rho} + b_Q(\theta_{\mathrm{P}},\omega)\Delta\left(\frac{1}{Q_{\mathrm{Pm}}}\right),
\end{aligned} \tag{18}$$

where

$$\begin{aligned}
a_M\left(\theta_{\mathrm{P}}\right) &= \frac{1}{4}\sec^2\theta_{\mathrm{P}}, \\
a_\mu\left(\theta_{\mathrm{P}}\right) &= -2\gamma\sin^2\theta_{\mathrm{P}}, \\
a_\rho\left(\theta_{\mathrm{P}}\right) &= \frac{\cos 2\theta_{\mathrm{P}}}{4\cos^2\theta_{\mathrm{P}}}, \\
a_Q\left(\theta_{\mathrm{P}},\omega\right) &= \frac{1}{2}\sec^2\theta_{\mathrm{P}}\frac{\psi\left(\omega\right)}{\pi} - 4\gamma\sin^2\theta_{\mathrm{P}}\frac{\psi\left(\omega\right)}{\pi h\left(\omega\right)}, \\
b_\mu\left(\theta_{\mathrm{P}}\right) &= \sqrt{\gamma}\sin\theta_{\mathrm{P}}\left(\frac{\sqrt{\gamma}\sin^2\theta_{\mathrm{P}}}{\sqrt{1-\gamma\sin^2\theta_{\mathrm{P}}}} - \cos\theta_{\mathrm{P}}\right), \\
b_\rho\left(\theta_{\mathrm{P}}\right) &= -\frac{\gamma\sin\theta_{\mathrm{P}}}{2\sqrt{1-\gamma\sin^2\theta_{\mathrm{P}}}}, \\
b_Q\left(\theta_{\mathrm{P}},\omega\right) &= \frac{2}{\pi}\sqrt{\gamma}\sin\theta_{\mathrm{P}}\left(\frac{\sqrt{\gamma}\sin^2\theta_{\mathrm{P}}}{\sqrt{1-\gamma\sin^2\theta_{\mathrm{P}}}} - \cos\theta_{\mathrm{P}}\right)\frac{\psi\left(\omega\right)}{h\left(\omega\right)},
\end{aligned} \tag{19}$$

in which $\gamma = \frac{\mu}{M}$, which indicates that we employ the ratio of S-to-P wave moduli at the reference frequency, γ, to replace the frequency-dependent moduli ratio $g\left(\omega\right)$.

Inversion of PP- and PSV-wave amplitudes for P- and S-wave moduli and P-wave maximum attenuation factor

We proceed to establishing an inversion approach of employing both PP-wave and PSV-wave amplitude variations with incidence angle and frequency (FAVA) to estimate P- and S-wave moduli and P-wave maximum attenuation factor. Before we estimate P- and S-wave moduli and attenuation factor, we first implement inversion for datasets of elastic impedance (EI) from partially stacked PP- and PSV-wave seismic data.

Using the derived PP- and PSV-wave reflection coefficients, we next explain how to derive PP- and PSV-wave elastic imepdances in terms of attenuation factor. We assume

$$d\left(\ln x\right) \approx \frac{\Delta x}{x}, \tag{20}$$

where x refers to EI, M, μ and ρ respectively, and we also employ the relationship

$$d\left(\frac{1}{Q_{\mathrm{Pm}}}\right) \approx \Delta\left(\frac{1}{Q_{\mathrm{Pm}}}\right), \tag{21}$$

under the assumption of small change in $\frac{1}{Q_{\mathrm{Pm}}}$ across the reflection interface.

Relationship between elastic impedance EI and reflection coefficient R is given by (Chen et al., 2014)

$$R \approx \frac{\Delta \mathrm{EI}}{2\mathrm{EI}}. \tag{22}$$

Combining equations (21)-(22), we obtain elastic impedances of PP-wave and PSV-wave, $\mathrm{EI_{PP}}$ and $\mathrm{EI_{PS}}$, which have differential forms:

$$\begin{aligned} d\left(\ln \mathrm{EI_{PP}}\right) =& 2a_M\left(\theta_{\mathrm{P}}\right) d\left(\ln M\right) + 2a_\mu\left(\theta_{\mathrm{P}}\right) d\left(\ln \mu\right) + 2a_\rho\left(\theta_{\mathrm{P}}\right) d\left(\ln \rho\right) + 2a_Q\left(\theta_{\mathrm{P}}, \omega\right) d\left(\frac{1}{Q_{\mathrm{Pm}}}\right), \\ d\left(\ln \mathrm{EI_{PS}}\right) =& 2b_\mu\left(\theta_{\mathrm{P}}\right) d\left(\ln \mu\right) + 2b_\rho\left(\theta_{\mathrm{P}}\right) d\left(\ln \rho\right) + 2b_Q\left(\theta_{\mathrm{P}}, \omega\right) d\left(\frac{1}{Q_{\mathrm{Pm}}}\right). \end{aligned} \tag{23}$$

Taking an integral on both sides of equation (23), we obtain final expressions of $\mathrm{EI_{PP}}$ and $\mathrm{EI_{PS}}$ after some algebra

$$\begin{aligned} \mathrm{EI_{PP}}\left(\theta_{\mathrm{P}}, \omega\right) =& M^{2a_M\left(\theta_{\mathrm{P}}\right)} \mu^{2a_\mu\left(\theta_{\mathrm{P}}\right)} \rho^{2a_\rho\left(\theta_{\mathrm{P}}\right)} \exp\left[2a_Q\left(\theta_{\mathrm{P}}, \omega\right)\left(\frac{1}{Q_{\mathrm{Pm}}}\right)\right], \\ \mathrm{EI_{PS}}\left(\theta_{\mathrm{P}}, \omega\right) =& \mu^{2b_\mu\left(\theta_{\mathrm{P}}\right)} \rho^{2b_\rho\left(\theta_{\mathrm{P}}\right)} \exp\left[2b_Q\left(\theta_{\mathrm{P}}, \omega\right)\left(\frac{1}{Q_{\mathrm{Pm}}}\right)\right]. \end{aligned} \tag{24}$$

Following Whitcombe (2002), we derive the normalized PP- and PSV-wave elastic impedances as

$$\begin{aligned} \mathrm{EI_{PP}}\left(\theta_{\mathrm{P}}, \omega\right) =& \mathrm{EI_{PP0}}\left(\frac{M}{M_0}\right)^{a_M\left(\theta_{\mathrm{P}}\right)} \left(\frac{\mu}{\mu_0}\right)^{a_\mu\left(\theta_{\mathrm{P}}\right)} \left(\frac{\rho}{\rho_0}\right)^{a_\rho\left(\theta_{\mathrm{P}}\right)} \exp\left[a_Q\left(\theta_{\mathrm{P}}, \omega\right)\left(\frac{1}{Q_{\mathrm{Pm}}}\right)\right], \\ \mathrm{EI_{PS}}\left(\theta_{\mathrm{P}}, \omega\right) =& \mathrm{EI_{PS0}}\left(\frac{\mu}{\mu_0}\right)^{b_\mu\left(\theta_{\mathrm{P}}\right)} \left(\frac{\rho}{\rho_0}\right)^{b_\rho\left(\theta_{\mathrm{P}}\right)} \exp\left[b_\mu\left(\theta_{\mathrm{P}}, \omega\right)\left(\frac{1}{Q_{\mathrm{Pm}}}\right)\right], \end{aligned} \tag{25}$$

where $\mathrm{EI_{PP0}} = \sqrt{M_0 \rho_0}$, $\mathrm{EI_{PS0}} = \sqrt{\mu_0 \rho_0}$, M_0, μ_0, and ρ_0 are constants of P- and S-wave moduli and density, which are provided by well log data.

In the case of N interface, relationships between PP- and PSV-wave elastic impedances and seismic data are given by

$$\begin{aligned} \mathbf{s}_{\mathrm{PP}}\left(\theta_{\mathrm{P}}, \omega\right) &= \mathbf{W}_{\mathrm{PP}}\, \mathbf{D}\, \mathbf{e}_{\mathrm{PP}}\left(\theta_{\mathrm{P}}, \omega\right), \\ \mathbf{s}_{\mathrm{PS}}\left(\theta_{\mathrm{P}}, \omega\right) &= \mathbf{W}_{\mathrm{PS}}\, \mathbf{D}\, \mathbf{e}_{\mathrm{PS}}\left(\theta_{\mathrm{P}}, \omega\right), \end{aligned} \tag{26}$$

where

$$\mathbf{s}_{\mathrm{PP}}\left(\theta_{\mathrm{P}}, \omega\right) = \begin{bmatrix} s^1_{\mathrm{PP}}\left(\theta_{\mathrm{P}}, \omega\right) \\ \vdots \\ s^N_{\mathrm{PP}}\left(\theta_{\mathrm{P}}, \omega\right) \end{bmatrix}, \mathbf{s}_{\mathrm{PS}}\left(\theta_{\mathrm{P}}, \omega\right) = \begin{bmatrix} s^1_{\mathrm{PS}}\left(\theta_{\mathrm{P}}, \omega\right) \\ \vdots \\ s^N_{\mathrm{PS}}\left(\theta_{\mathrm{P}}, \omega\right) \end{bmatrix},$$

$$\mathbf{D} = \begin{bmatrix} -\frac{1}{2} & \frac{1}{2} & & & \\ & -\frac{1}{2} & \frac{1}{2} & & \\ & & \ddots & \ddots & \\ & & & -\frac{1}{2} & \frac{1}{2} \end{bmatrix},$$

$$
\begin{aligned}
\mathbf{W}_{\mathrm{PP}} &= \begin{bmatrix} w_{\mathrm{PP}}^{1} & 0 & \dots & 0 \\ w_{\mathrm{PP}}^{2} & w_{\mathrm{PP}}^{1} & \ddots & \vdots \\ \vdots & \vdots & \ddots & 0 \\ w_{\mathrm{PP}}^{N} & w_{\mathrm{PP}}^{N-1} & \dots & w_{\mathrm{PP}}^{1} \end{bmatrix}, \\
\mathbf{W}_{\mathrm{PS}} &= \begin{bmatrix} w_{\mathrm{PS}}^{1} & 0 & \dots & 0 \\ w_{\mathrm{PS}}^{2} & w_{\mathrm{PS}}^{1} & \ddots & \vdots \\ \vdots & \vdots & \ddots & 0 \\ w_{\mathrm{PS}}^{N} & w_{\mathrm{PS}}^{N-1} & \dots & w_{\mathrm{PS}}^{1} \end{bmatrix}, \\
\mathbf{e}_{\mathrm{PP}}\left(\theta_{\mathrm{P}}, \omega\right) &= \begin{bmatrix} \ln \mathrm{EI}_{\mathrm{PP}}^{1}\left(\theta_{\mathrm{P}}, \omega\right) \\ \vdots \\ \ln \mathrm{EI}_{\mathrm{PP}}^{N+1}\left(\theta_{\mathrm{P}}, \omega\right) \end{bmatrix}, \\
\mathbf{e}_{\mathrm{PS}}\left(\theta_{\mathrm{P}}, \omega\right) &= \begin{bmatrix} \ln \mathrm{EI}_{\mathrm{PS}}^{1}\left(\theta_{\mathrm{P}}, \omega\right) \\ \vdots \\ \ln \mathrm{EI}_{\mathrm{PS}}^{N+1}\left(\theta_{\mathrm{P}}, \omega\right) \end{bmatrix},
\end{aligned} \tag{27}
$$

in which $s_{\mathrm{PP}}^{1} \dots s_{\mathrm{PP}}^{N}$ and $s_{\mathrm{PS}}^{1} \dots s_{\mathrm{PS}}^{N}$ represent elements of PP- and PSV-wave seismic data, $w_{\mathrm{PP}}^{1} \dots w_{\mathrm{PP}}^{N}$ and $w_{\mathrm{PS}}^{1} \dots w_{\mathrm{PS}}^{N}$ represent elements of wavelets extracted from input PP- and PSV-wave seismic data, $\ln \mathrm{EI}_{\mathrm{PP}}^{1} \dots \ln \mathrm{EI}_{\mathrm{PP}}^{N+1}$ and $\ln \mathrm{EI}_{\mathrm{PS}}^{1} \dots \ln \mathrm{EI}_{\mathrm{PS}}^{N+1}$ represent elements of logarithmic elastic impedances of PP- and PSV-wave, and $\mathbf{D}$ is a $N \times (N+1)$ differential matrix.

Following Chen et al. (2018), we employ a model-constrained and damping least-squares algorithm to estimate $\mathrm{EI}_{\mathrm{PP}}$ and $\mathrm{EI}_{\mathrm{PS}}$ respectively using frequency-components extracted from PP- and PSV-wave seismic data that are partially stacked over different ranges of incidence angle, which are used as input datasets for estimation of P- and S-wave moduli and attenuation factor. The solution is given by

$$
\begin{aligned}
\mathbf{e}_{\mathrm{PP}}\left(\theta_{\mathrm{P}l}, \omega_k\right) =& \mathbf{e}_{\mathrm{PP}}^{\mathrm{mod}}\left(\theta_{\mathrm{P}l}, \omega_k\right) \\
&+ \left(\mathbf{L}_{\mathrm{PP}}^{\dagger}\, \mathbf{L}_{\mathrm{PP}} + \sigma_{\mathrm{P}} \mathbf{I}\right)^{-1} \mathbf{L}_{\mathrm{PP}}^{\dagger} \left[\mathbf{s}_{\mathrm{PP}}\left(\theta_{\mathrm{P}l}, \omega_k\right) - \mathbf{L}_{\mathrm{PP}}\, \mathbf{e}_{\mathrm{PP}}^{\mathrm{mod}}\left(\theta_{\mathrm{P}l}, \omega_k\right)\right], \\
\mathbf{e}_{\mathrm{PS}}\left(\theta_{\mathrm{P}l}, \omega_k\right) =& \mathbf{e}_{\mathrm{PS}}^{\mathrm{mod}}\left(\theta_{\mathrm{P}l}, \omega_k\right) \\
&+ \left(\mathbf{L}_{\mathrm{PS}}^{\dagger}\, \mathbf{L}_{\mathrm{PS}} + \sigma_{\mathrm{S}} \mathbf{I}\right)^{-1} \mathbf{L}_{\mathrm{PS}}^{\dagger} \left[\mathbf{s}_{\mathrm{PS}}\left(\theta_{\mathrm{P}l}, \omega_k\right) - \mathbf{L}_{\mathrm{PS}}\, \mathbf{e}_{\mathrm{PS}}^{\mathrm{mod}}\left(\theta_{\mathrm{P}l}, \omega_k\right)\right],
\end{aligned} \tag{28}
$$

where $\mathbf{L}_{\mathrm{PP}} = \mathbf{W}_{\mathrm{PP}}\, \mathbf{D}$, $\mathbf{L}_{\mathrm{PS}} = \mathbf{W}_{\mathrm{PS}}\, \mathbf{D}$, $\mathbf{e}_{\mathrm{PP}}^{\mathrm{mod}}\left(\theta_{\mathrm{P}l}, \omega_k\right)$ and $\mathbf{e}_{\mathrm{PS}}^{\mathrm{mod}}\left(\theta_{\mathrm{P}l}, \omega_k\right)$ are initial models, σ_{P} and σ_{S} are damping factors, $\mathbf{L}_{\mathrm{PP}}^{\dagger}$ and $\mathbf{L}_{\mathrm{PS}}^{\dagger}$ are transpose matrices of $\mathbf{L}_{\mathrm{PP}}$ and $\mathbf{L}_{\mathrm{PS}}$, $\mathbf{I}$ is a unit matrix. The variable $\theta_{\mathrm{P}l}$ respectively represents small-, middle- and large-incidence angels (i.e. $\theta_{\mathrm{P}1}$, $\theta_{\mathrm{P}2}$ and $\theta_{\mathrm{P}3}$), and ω_k represents dominant frequencies of input frequency components.

With the estimated results of PP- and PSV- wave elastic impedances in hand, we proceed to the prediction of unknown parameter vector that involves P- and S-wave moduli,

density and P-wave maximum attenuation factor. Relationship between the vector of EI datasets $\mathbf{d}$ and the unknown parameter vector $\mathbf{m}$ is given by

$$\mathbf{d} = \mathbf{G}\left(\mathbf{m}\right), \tag{29}$$

where

$$\mathbf{d} = \begin{bmatrix} \mathbf{e}_{\mathrm{PP}} \\ \mathbf{e}_{\mathrm{PS}} \end{bmatrix},$$
$$\mathbf{m} = \begin{bmatrix} M \\ \mu \\ \rho \\ 1/Q_{\mathrm{Pm}} \end{bmatrix}, \tag{30}$$

and $\mathbf{G}$ is an operator related to incidence angle and frequency. Given an unknown parameter vector, we use equation 25 to compute PP- and PSV-wave elastic impedances.

In order to predict the unknown parameter vector $\mathbf{m}$, we employ the main strategy of full waveform inversion (FWI) to estimate perturbation in unknown parameter vector (i.e. $\Delta\mathbf{m}$) rather than to directly invert for $\mathbf{m}$. The solution of $\mathbf{m}$ is given by (Köhn, 2011; Pan et al., 2015; Geng et al., 2018)

$$\mathbf{m} = \mathbf{m}_0 + \boldsymbol{\zeta}\Delta\mathbf{m}, \tag{31}$$

where $\mathbf{m}_0$ is initial guess of unknown parameter vector, and $\boldsymbol{\zeta}$ is the vector of step length. The calculation of perturbation is expressed as (Köhn, 2011)

$$\Delta\mathbf{m} = -\mathbf{H}^{-1}\mathbf{Y}, \tag{32}$$

where

$$\mathbf{H} \approx \mathbf{Y}\mathbf{Y}^{\dagger}, \tag{33}$$

$$\mathbf{Y} = \frac{\partial \mathbf{d}_{\mathrm{mod}}}{\partial \mathbf{m}}\left(\mathbf{d}_{\mathrm{obs}} - \mathbf{d}_{\mathrm{mod}}\right), \tag{34}$$

where $\mathbf{d}_{\mathrm{obs}}$ is the vector of observed data (i.e. the estimated elastic impedance in the previous step), $\mathbf{d}_{\mathrm{mod}}$ is the vector of synthetic data using a model vector $\mathbf{m}_{\mathrm{mod}}$, and

$$\frac{\partial \mathbf{d}_{\mathrm{mod}}}{\partial \mathbf{m}} = \left.\frac{\partial \mathbf{EI}}{\partial \mathbf{m}}\right|_{\mathbf{m}=\mathbf{m}_{\mathrm{mod}}} = \begin{bmatrix} \frac{\partial \mathrm{EI}_{\mathrm{PP}}}{\partial M} \\ \frac{\partial \mathrm{EI}_{\mathrm{PP}}}{\partial \mu} \\ \frac{\partial \mathrm{EI}_{\mathrm{PP}}}{\partial \rho} \\ \frac{\partial \mathrm{EI}_{\mathrm{PP}}}{\partial (1/Q_{\mathrm{Pm}})} \\ \frac{\partial \mathrm{EI}_{\mathrm{PS}}}{\partial M} \\ \frac{\partial \mathrm{EI}_{\mathrm{PS}}}{\partial \mu} \\ \frac{\partial \mathrm{EI}_{\mathrm{PS}}}{\partial \rho} \\ \frac{\partial \mathrm{EI}_{\mathrm{PS}}}{\partial (1/Q_{\mathrm{Pm}})} \end{bmatrix}_{\mathbf{m}=\mathbf{m}_{\mathrm{mod}}}. \tag{35}$$

Based on the derived formulas of PP- and PSV-wave elastic impedances (equation 25), we may compute the derivation of $\mathbf{d}_{\mathrm{mod}}$ with respect to $\mathbf{m}$. We employ PP- and PSV-wave EI results of each incidence angle and each frequency to implement the inversion for the unknown parameter vector, and we preserve the average value of all the estimated unknown parameter vectors as the final inversion result.

Construction of initial guess of unknown parameter vector

Equation (31) reveals that in order to obtain the final solution of unknown parameter vector involving P- and S-wave moduli and P-wave maximum attenuation factor, an acceptable initial model of unknown parameter vector, $\mathbf{m}_0$, is required. For synthetic tests, we utilize curves of P- and S-wave velocities and density provided by well log to compute P- and S-wave moduli, and smoothed versions of computed results are used as initial values of P- and S-wave moduli. In order to obtain initial guess of P-wave attenuation factor, we employ relationship between attenuation factor and elastic parameters (e.g. P- and S-wave velocities and density) to construct the curve of attenuation factor. Using a function proposed by Margrave (2013), we compute the curve of attenuation factor using P-wave velocity and density provided by well log. The function is given by (Margrave, 2013)

$$\frac{1}{Q_{\mathrm{Pm}}} \approx \left(\frac{1}{Q_{\mathrm{P}}}\right)_{\alpha} + \left(\frac{1}{Q_{\mathrm{P}}}\right)_{\rho}, \tag{36}$$

where $\left(\frac{1}{Q_{\mathrm{P}}}\right)_{\alpha}$ and $\left(\frac{1}{Q_{\mathrm{P}}}\right)_{\rho}$ represent attenuation factors computed using P-wave velocity and density respectively, which are computed as (Margrave, 2013)

$$\begin{aligned} \left(\frac{1}{Q_{\mathrm{P}}}\right)_{\alpha} &= 1/\left[Q_0 \frac{\alpha(z)-\alpha_1}{\alpha_0-\alpha_1} + Q_1 \frac{\alpha(z)-\alpha_0}{\alpha_1-\alpha_0}\right] \\ \left(\frac{1}{Q_{\mathrm{P}}}\right)_{\rho} &= 1/\left[Q_0 \frac{\rho(z)-\rho_1}{\rho_0-\rho_1} + Q_1 \frac{\rho(z)-\rho_0}{\rho_1-\rho_0}\right], \end{aligned} \tag{37}$$

where Q_0, Q_1, α_0, α_1, ρ_0, and ρ_1 are special constants that determine the linear relationships, and z represents different samples. Following Chen et al. (2018), we assume Q_0 and Q_1 to be 2 and 80 respectively in the present study, which corresponds to maximum and minimum values of P-wave attenuation factor.

In the case of real data inversion, we may roughly estimate P- and S-wave velocities and density using pre-stack seismic amplitude data, and then we obtain rough results of P- and S-wave moduli. The smoothed version of rough result is used as initial model. Again using the function proposed by Margrave (2013), we roughly compute P-wave maximum attenuation factor, and the smoothed version of computed results is used as initial guess of P-wave maximum attenuation factor.

NUMERICAL EXAMPLES

Verification of robustness and stability

We first utilize a well log model to verify robustness and stability of the proposed inversion approach. Combining equations (36) and (37), we first use P-wave velocity and density to compute P-wave maximum attenuation factor. Figure 2 plots curves of P- and S-wave velocities, density and the constructed attenuation factor. Given Ricker wavelets of different dominant frequencies ($f_1 = 14\mathrm{Hz}$ and $f_2 = 28\mathrm{Hz}$), we generate PP- and PSV-wave synthetic seismic data of frequencies f_1 and f_2 in the case of angle range $1^\circ - 33^\circ$ using the derived reflection coefficients. Figure 3 plots profiles of generated PP- and PSV-wave seismic data, in which we added Gaussian random noise to obtain noisy seismic data of different signal-to-noise ratios (SNRs).

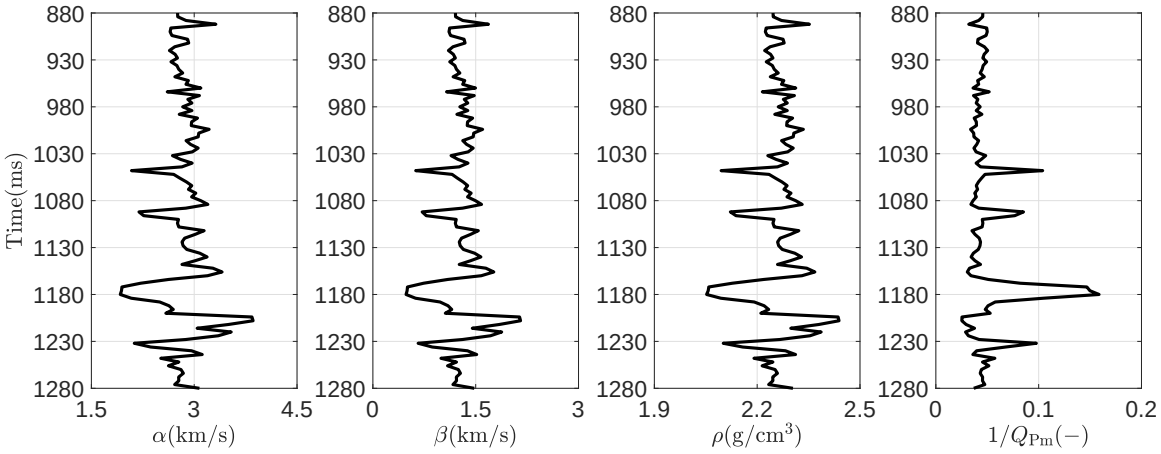

FIG. 2. A well log model: curves of P- and S-wave velocities, density and constructed P-wave maximum attenuation factor. Quantities used for constructing P-wave maximum attenuation factor are $Q_0 = 2$, $Q_1 = 80$, $\alpha_0 = 1.55$ km/s, $\alpha_1 = 3.85$ km/s, $\rho_0 = 2.0$ g/cm^3, $\rho_1 = 2.45$ g/cm^3.

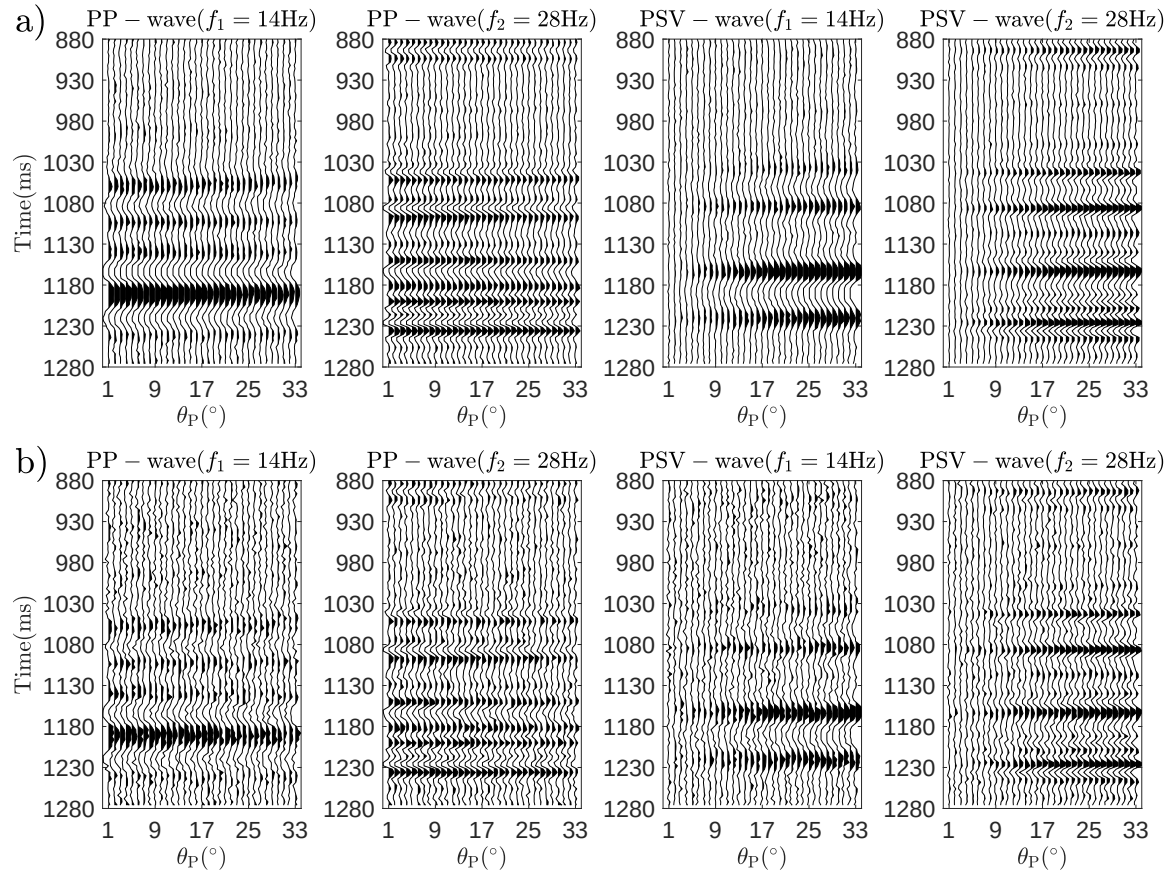

FIG. 3. Noisy synthetic PP- and PSV-wave seismic data of different frequencies $f_1 = 14$Hz and $f_2 = 28$Hz. a) SNR=5, and b) SNR=2.

As outlined in the previous section, we first implement the inversion for PP- and PSV-wave elastic impedances, and the input data are PP- and PSV-wave partially-incidence-stacked data, which are constructed stacking the synthetic PP- and PSV-wave data over different ranges of incidence angle, i.e. the small-incidence-angle ($\theta_{\mathrm{P1}} = 6^\circ$) data are

stacked over the angle range $1^\circ - 11^\circ$; the middle-incidence-angle ($\theta_{\mathrm{P2}} = 17^\circ$) data are stacked over the angle range $12^\circ - 22^\circ$; and the large-incidence-angle ($\theta_{\mathrm{P3}} = 28^\circ$) data are stacked over the angle range $23^\circ - 33^\circ$. Figure 4 plots comparisons between inversion results and true values of logarithmic elastic impedances of PP-wave and PSV-wave, and true values of logarithmic EI are computed using equation 25. We observe that there is a good match between true value and inversion result of logarithmic elastic impedance for both PP-wave and PSV-wave in the case of different frequencies and incidence angles. It indicates that the inversion results of PP- and PSV-wave elastic impedances obtained using the model-constrained and damping least-squares algorithm can be used as the input datasets for estimating P- and S-wave moduli and attenuation factor.

With the estimated PP- and PSV-wave elastic impedances in hand, we next implement the estimation of P- and S-wave moduli and P-wave maximum attenuation factor using the inversion approach proposed in the previous section. Figure 5 plots comparisons between inversion results and true values of unknown parameters (i.e. P- and S-wave moduli and P-wave maximum attenuation factor) in the case of SNRs of 5 and 2 respectively, and Figure 6 plot relatively errors computed using inversion results and true values (e.g., $\varepsilon_M = M_{\mathrm{inverterd}} - M_{\mathrm{true}}$).

In Figures 5 and 6 we observe that the final inversion result (i.e. average value of all the estimated results) can match the true value closely with only small errors even in the case of $\mathrm{SNR}\geq 2$, which confirms that the proposed inversion approach is stable and robust.

Example of real data

We proceed to applying the proposed approach to real data that are acquired over an oil-bearing reservoir to further verify its stability and reliability. Figure 7 plot PP- and PSV-wave angle gathers, which have undergone amplitude compliant processing and horizon matching using a commercial software package. We observe that around the location of horizon H_1 P-wave velocity exhibits relatively low values, and phenomenons of PP- and PSV-wave amplitudes varying with P-wave incidence angle (AVA) occur.

Figure 8 plots frequency components ($f_1 = 5\mathrm{Hz}$ and $f_2 = 12\mathrm{Hz}$) extracted from partially-incidence-stacked PP- and PSV-wave seismic data, and the processing of partially-incidence-stack is implemented as:

- Seismic data of small incidence angle ($\theta_{\mathrm{P1}} = 7^\circ$) are stacked over the angle range $3^\circ - 10^\circ$;
- Seismic data of middle incidence angle ($\theta_{\mathrm{P2}} = 15^\circ$) are stacked over the angle range $11^\circ - 18^\circ$;
- Seismic data of large incidence angle ($\theta_{\mathrm{P3}} = 23^\circ$) are stacked over the angle range $19^\circ - 26^\circ$.

We emphasize that the frequency components are obtained using two rectangle filters; i.e., we employ the rectangle filter of frequency range 2Hz-8Hz and that of frequency range

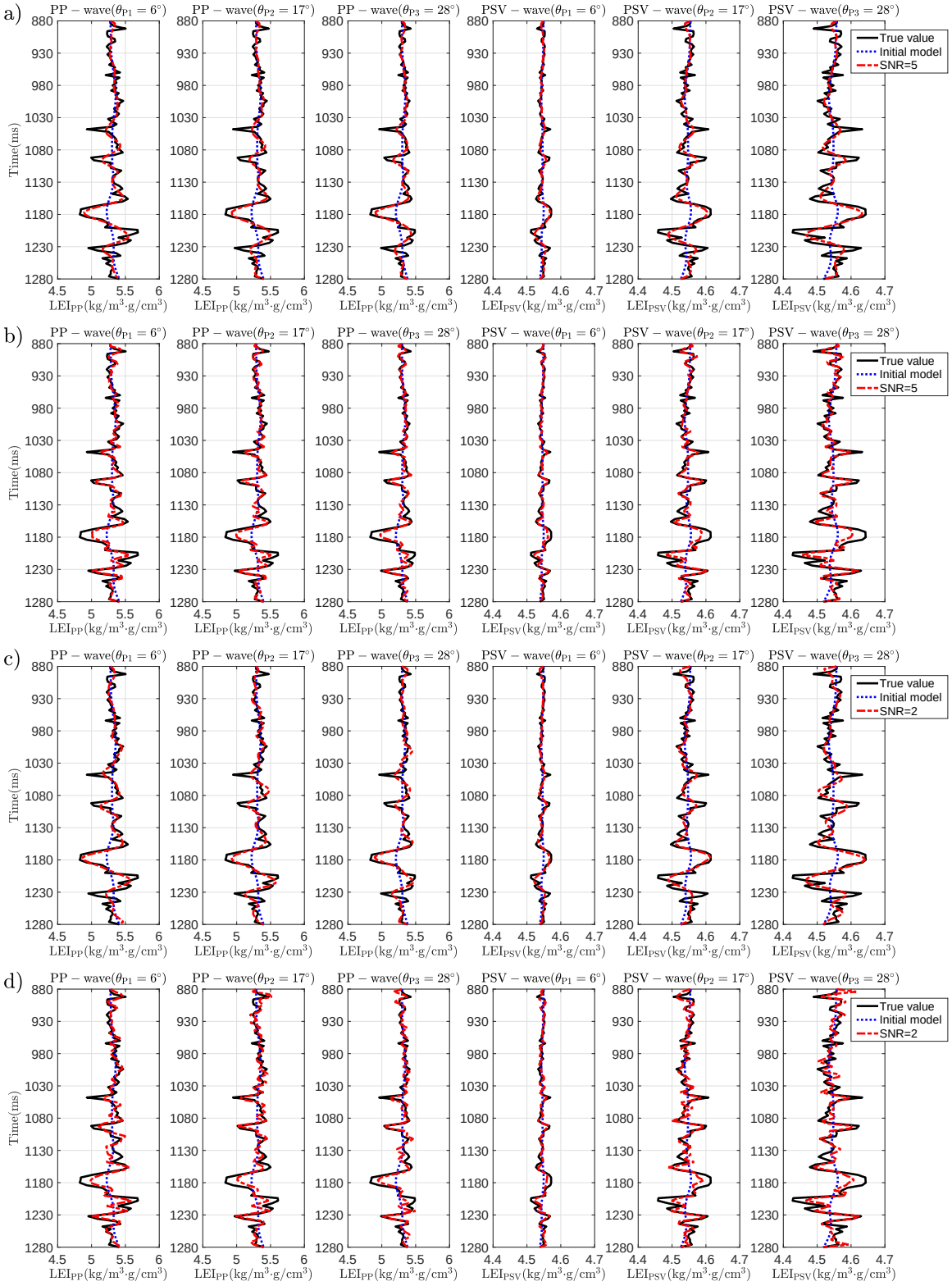

FIG. 4. Comparisons between inversion results and true values of logarithmic PP- and PSV-wave elastic impedances. a) and c) Comparisons between inversion results of SNRs of 5 and 2 and true values for the case of f_1 of 14Hz; b) and d) Comparisons between inversion results of SNRs of 5 and 2 and true values for the case of f_2 of 28Hz.

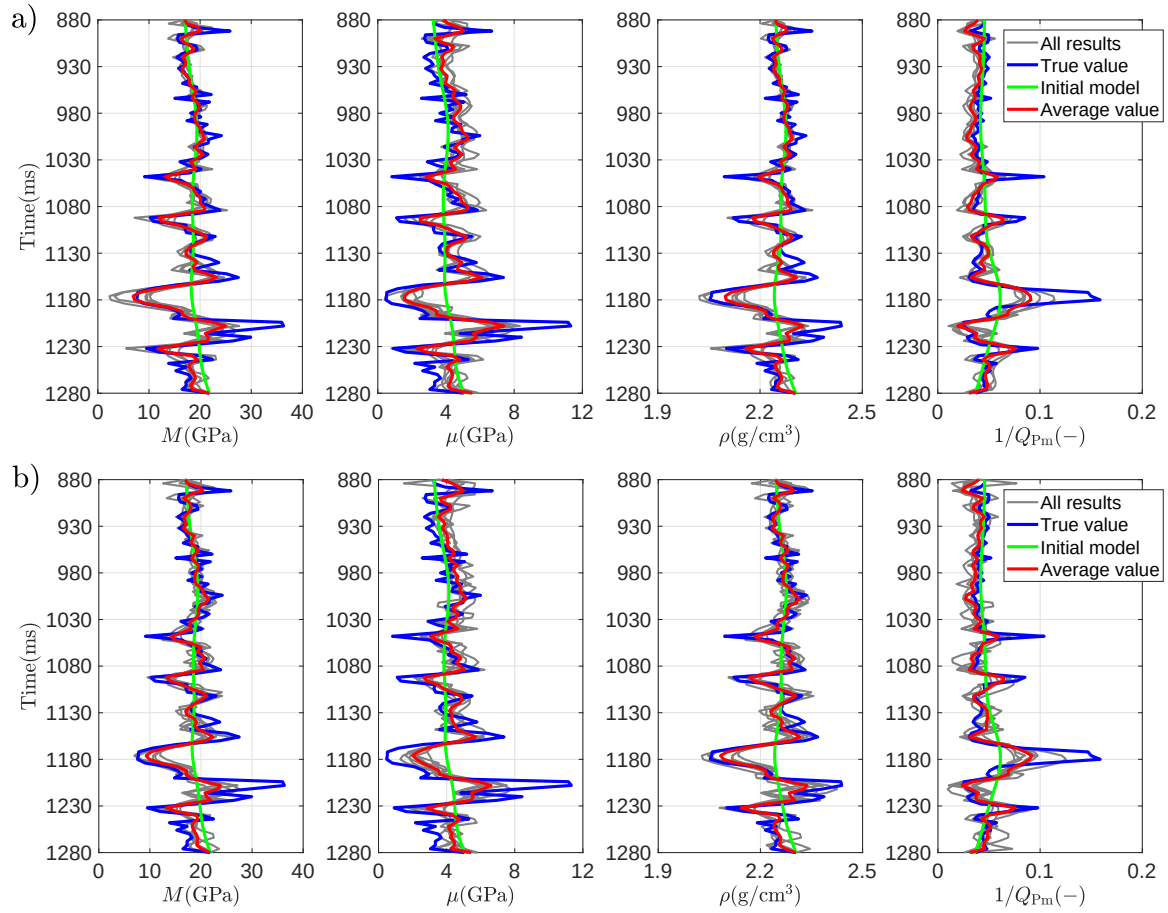

FIG. 5. Comparisons between inversion results and true values of P- and S-wave moduli, density and P-wave maximum attenuation factor. Blue and red curves respectively represent true values and inversion results of P- and S-wave moduli, density and P-wave maximum attenuation factor. Grey curves represent inversion results obtained using elastic impedances of different frequencies and incidence angles. The green curve represents the initial model, which is the smoothed version of true value. a) SNR=5; b) SNR=2.

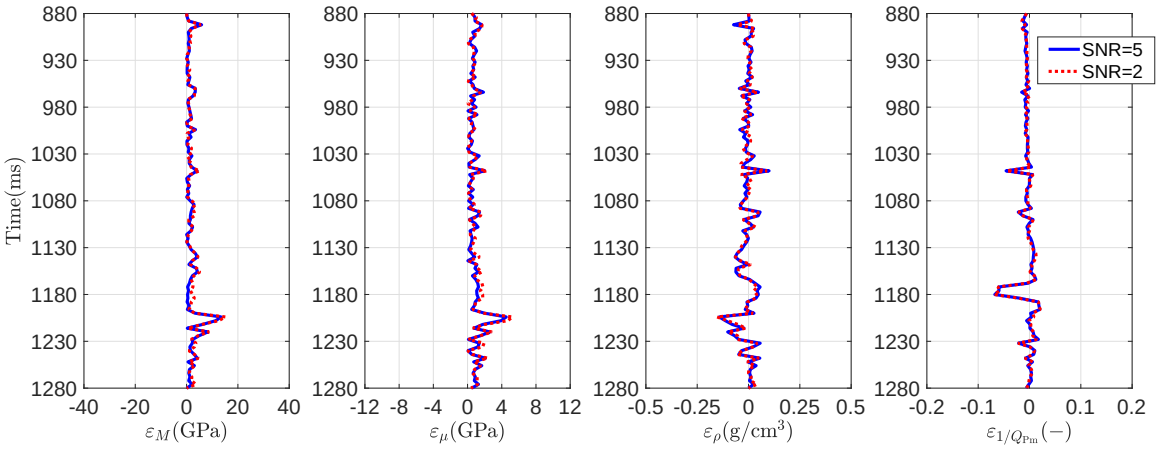

FIG. 6. Errors between inversion results and true values (e.g., $\varepsilon_M = M_{\mathrm{inverterd}} - M_{\mathrm{true}}$).

9Hz-15Hz to respectively obtain the data of dominant frequency $f_1 = 5$Hz and those of dominant frequency $f_2 = 12$Hz. Wavelets extracted from these frequency components

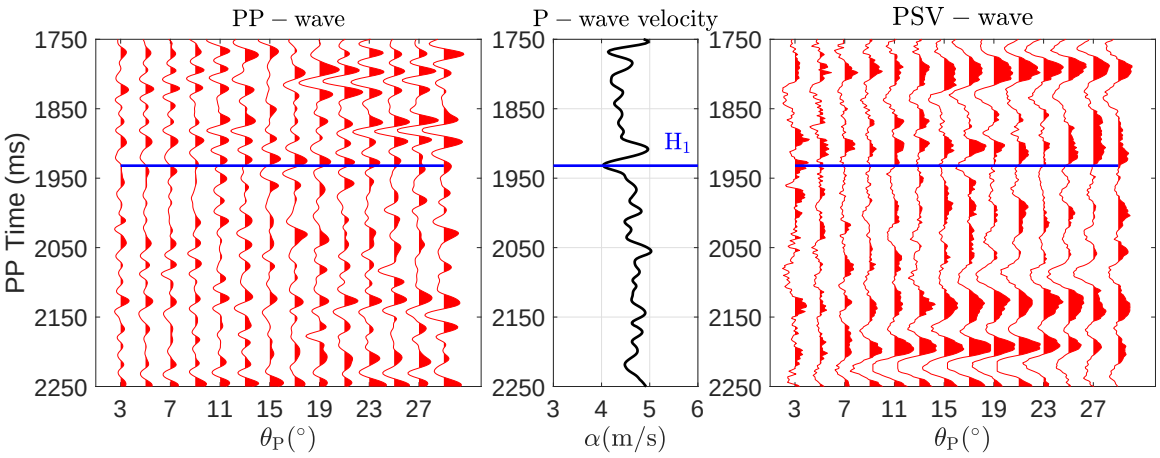

FIG. 7. PP- and PSV-wave angle gathers, and P-wave velocity curve provided by well log.

are displayed in Figure 9. We again utilize the model-constrained and damping least-squares algorithm outlined in the previous section to estimate results of PP- and PSV-wave impedances, which will be input datasets for the prediction of P- and S-wave moduli, density and P-wave attenuation factor. Figure 10 plots initial models of PP- and PSV-wave elastic impedances that are constructed using well log data, which will be employed for constraining the estimation of PP- and PSV-wave impedances. In Figure 11 we plot results of PP- and PSV-wave elastic impedances estimated using the least-squares algorithm. We observe that around the location of oil-bearing (marked by the dashed ellipse) PP-wave elastic impedances exhibit relatively low values, and PSV-wave elastic impedances exhibit relatively high values.

With the estimated PP- and PSV-wave EI datasets in hand, we proceed to the prediction of P- and S-wave moduli, density and P-wave attenuation factor using the proposed inversion approach. We again employ the commercial software package to implement the AVA inversion for P- and S-wave velocities and density, which are used to roughly compute P- and S-wave moduli, and their smoothed versions are utilized as initial models for the inversion. We stress that the initial model of P-wave attenuation factor is also a smoothed version of attenuation factor calculated using the inverted P-wave velocity and density based on the function proposed by Margrave (2013). Figure 12 plots the constructed initial models of P- and S-wave moduli, density and P-wave attenuation factor.

Utilizing the estimated PP- and PSV-wave elastic impedances of different frequencies and incidence angles one by one to implement the inversion for unknown parameters, we compute the average result of the unknown parameter using all the inverted results. Final inversions results of P- and S-wave moduli, density and P-wave attenuation factor are plotted in Figure 13. We observe that around the location of oil-bearing reservoirs the inverted P- and S-wave moduli and density exhibit relatively high values; however the P-wave attenuation factor shows a relatively high value. We next compare the inversion results of P- and S-wave moduli, density and P-wave attenuation factor extracted at CDP650 with those computed using well log data, as plotted in Figure 14. We observe that there is a good match between the inversion results and the well log curves, which confirms the proposed approach may generate reliable results of P- and S-wave moduli, density and attenuation

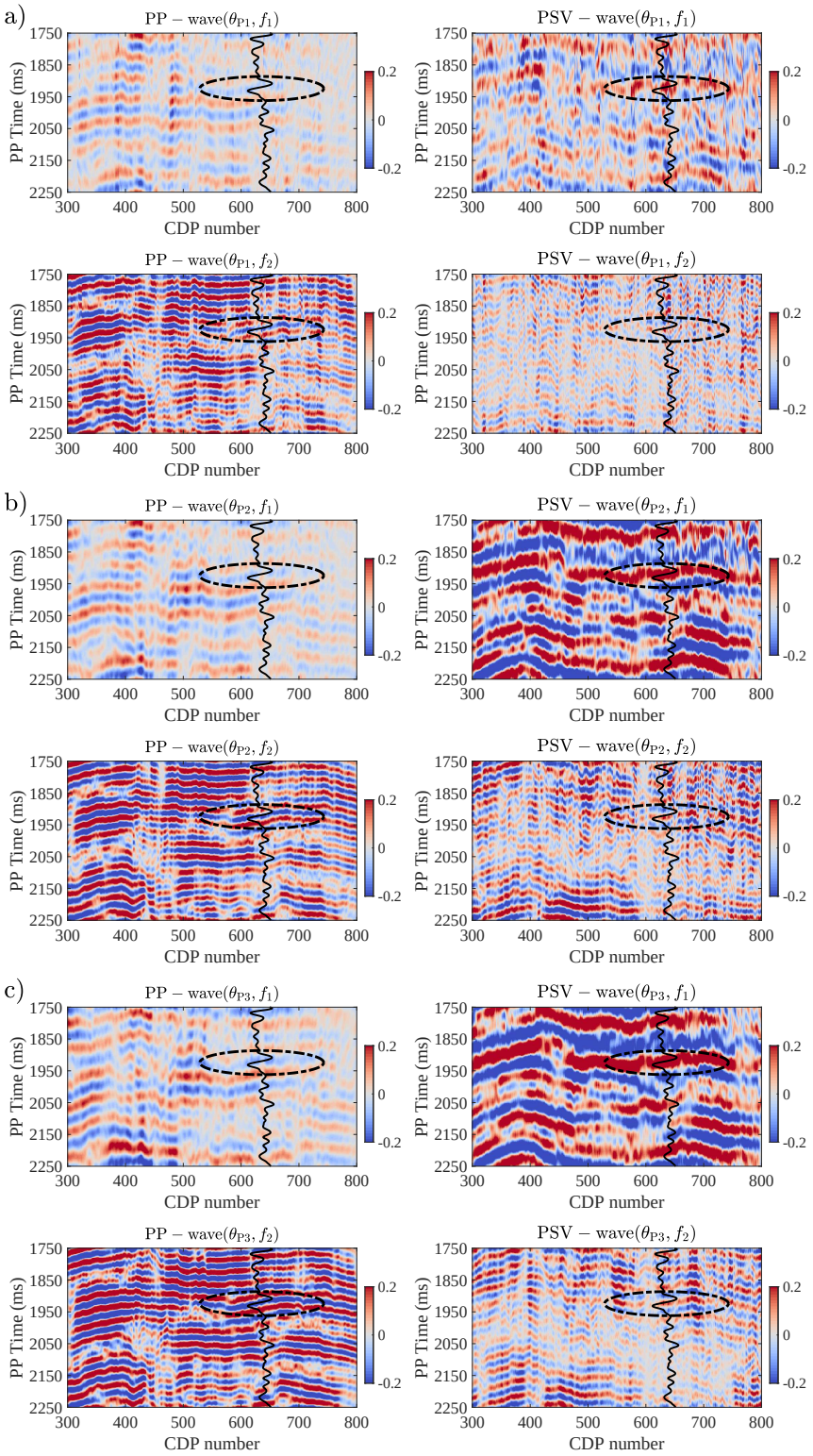

FIG. 8. Frequency components of partially-incidence-stacked seismic data. a) PP- and PSV-wave data of small incidence angle $\theta_{\mathrm{P1}} = 7°$; b) PP- and PSV-wave data of middle incidence angle $\theta_{\mathrm{P2}} = 15°$; and c) PP- and PSV-wave data of large incidence angle $\theta_{\mathrm{P3}} = 23°$. Dominant frequencies are $f_1 = 5\mathrm{Hz}$ and $f_2 = 12\mathrm{Hz}$. Dashed ellipse indicates the location of oil-bearing reservoir. Black curve represents P-wave velocity provided by well log.

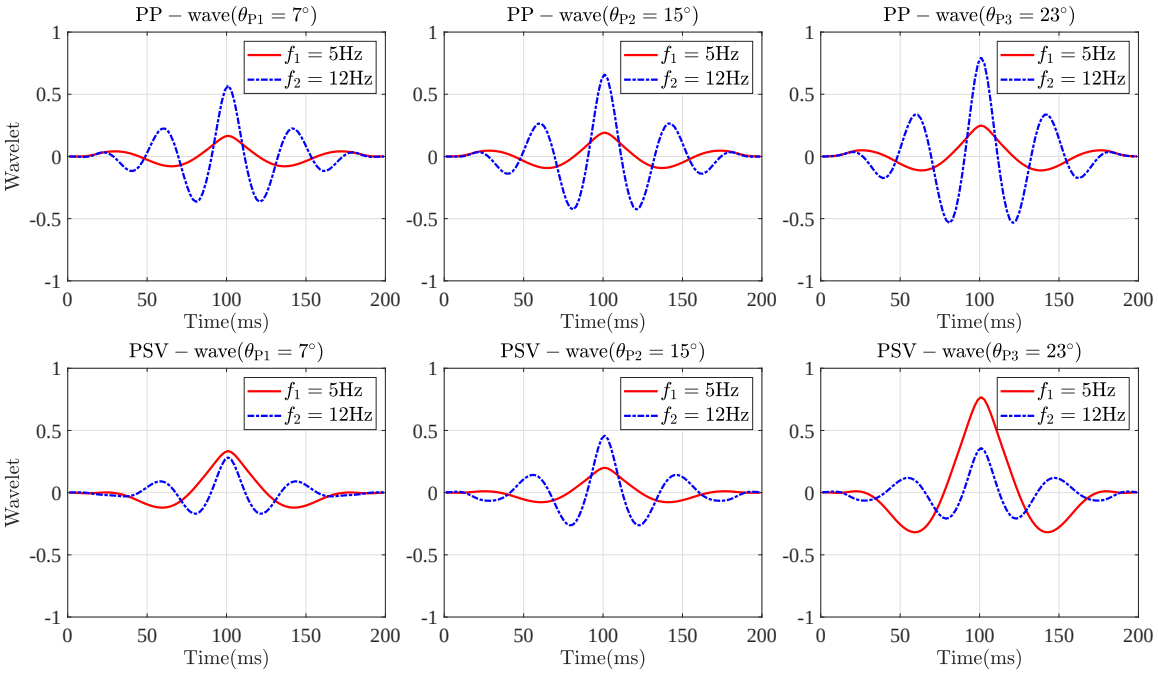

FIG. 9. Seismic wavelets extracted from frequency components.

factor.

CONCLUSIONS

Beginning with re-expressions of P- and S-wave velocities and moduli in anelastic media, we derive PP- and PSV-wave approximate and linearized reflection coefficients and anelastic impedances as a function of P-wave maximum attenuation factor by solving Zoeppritz equations. Based on the derived reflection coefficients and anelastic impedances, we propose an inversion approach and workflow of utilizing PP- and PSV-wave anelastic impedances that are estimated from partially-incidence-angle stacked seismic data using a least-squares inversion algorithm to predict unknown parameters involving P- and S-wave moduli, density and P-wave attenuation factor. Results of full Newton step are computed using both PP- and PSV-wave anelastic impedances, and final inversion results of unknown parameters are average values that combine initial models and all the computed Newton step. We stress that the initial model of P-wave attenuation factor is constructed using P-wave velocity and density. We first apply the proposed inversion approach to synthetic data of signal-to-noise ratio (SNR) of 5 and 2 to verify its stability and robustness, and then we utilize the real data acquired over an oil-bearing reservoir to testify the reliability of the inversion approach. We conclude that P- and S-wave moduli and P-wave attenuation factor are estimated stably in the case of seismic data of a moderate SNR; and following the inversion workflow reliable we may obtain reliable attenuation factor, which provides additional and valuable result for fluid identification.

ACKNOWLEDGMENTS

We thank the sponsors of CREWES for continued support. This work was funded by CREWES industrial sponsors, and NSERC (Natural Science and Engineering Research

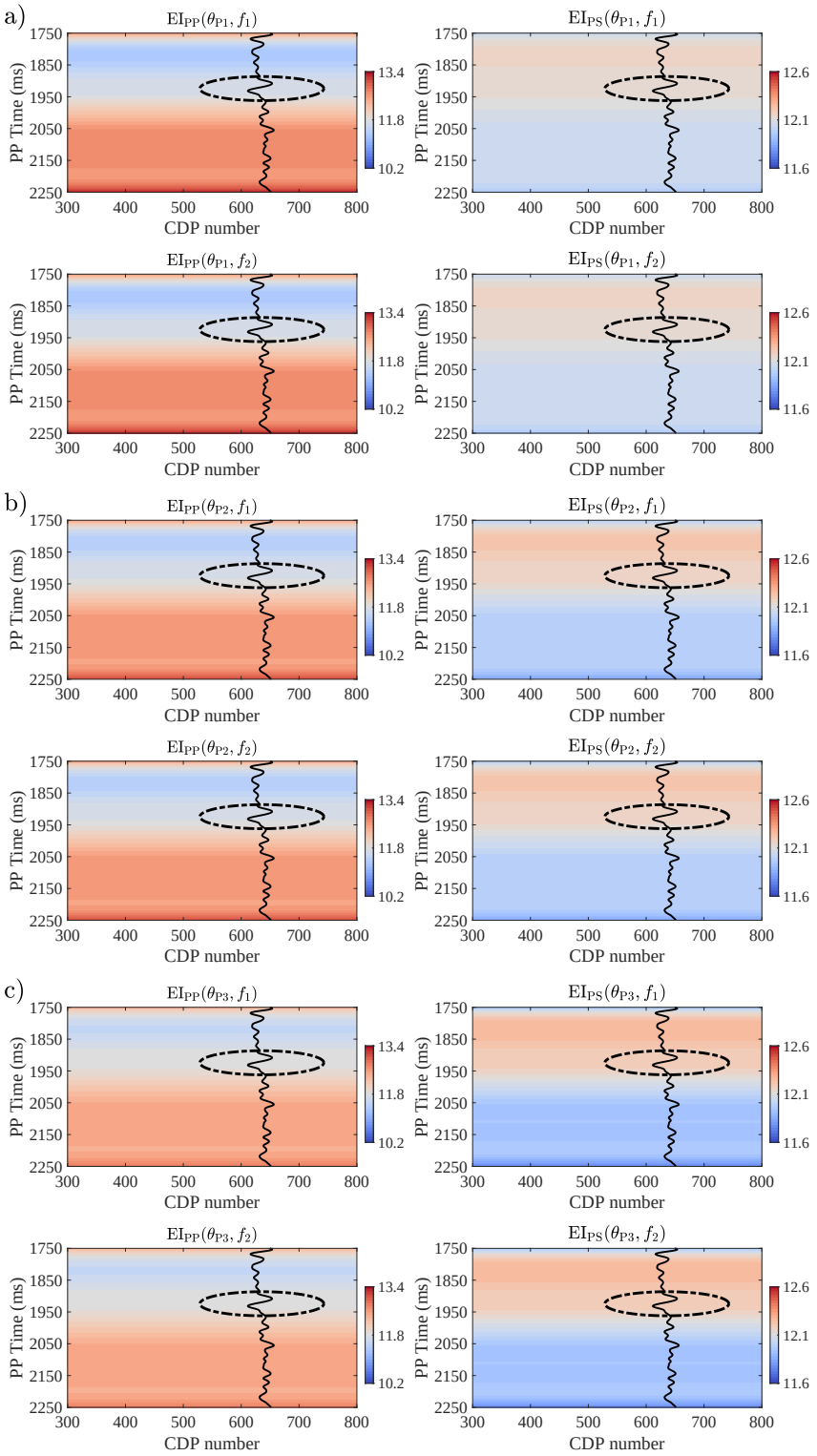

FIG. 10. Initial models constructed for constraining the estimation of PP- and PSV-wave elastic impedances. P-wave incidence angles are $\theta_{\mathrm{P1}} = 7°$, $\theta_{\mathrm{P2}} = 15°$, and $\theta_{\mathrm{P3}} = 23°$. Dominant frequencies are $f_1 = 5\mathrm{Hz}$, and $f_2 = 12\mathrm{Hz}$. Dashed ellipse indicates the location of oil-bearing reservoir. Black curve represents P-wave velocity provided by well log.

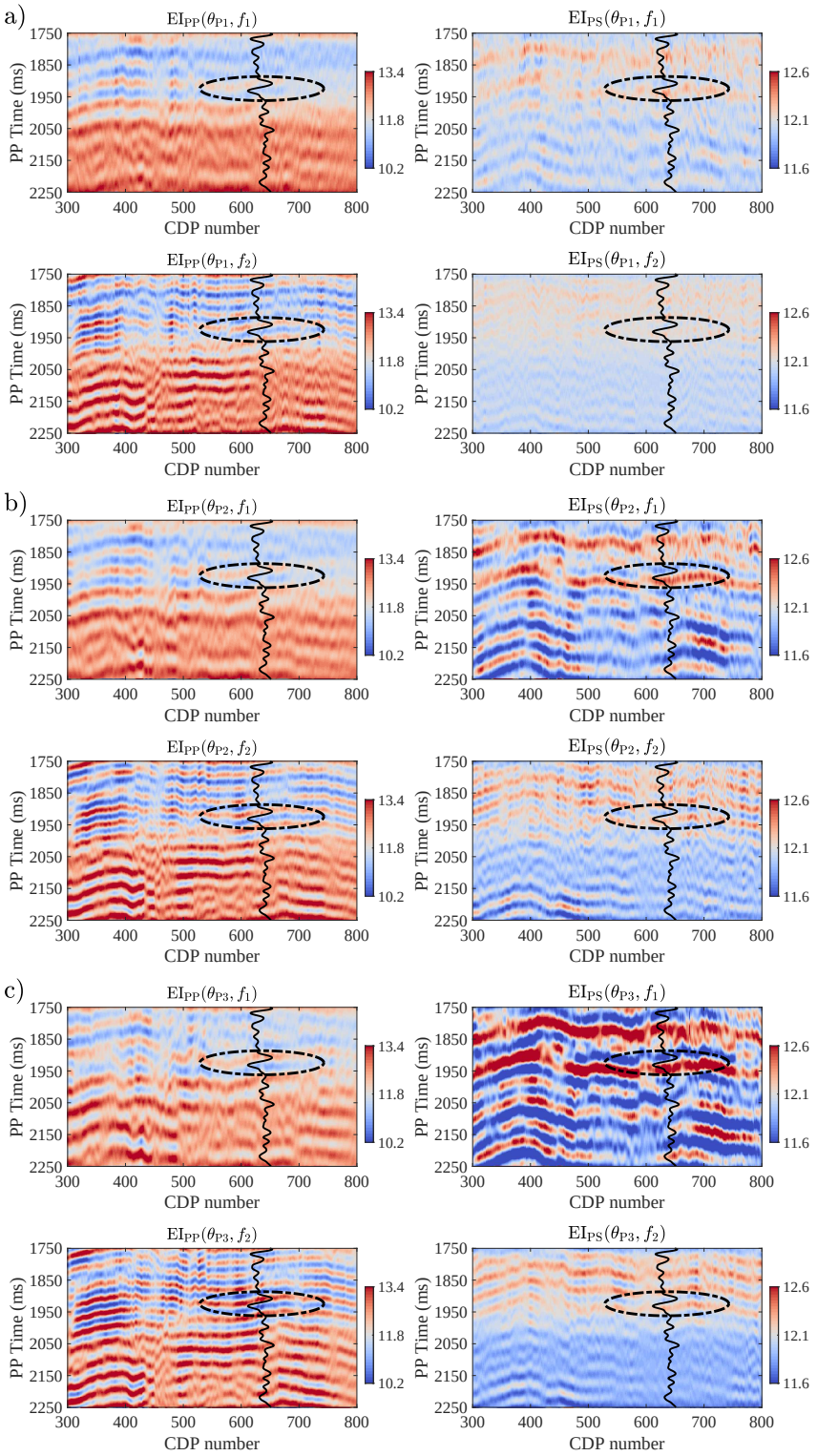

FIG. 11. Inversion results of PP- and PSV-wave elastic impedances. P-wave incidence angles are $\theta_{\mathrm{P1}} = 7°$, $\theta_{\mathrm{P2}} = 15°$, and $\theta_{\mathrm{P3}} = 23°$. Dominant frequencies are $f_1 = 5\mathrm{Hz}$, and $f_2 = 12\mathrm{Hz}$. Dashed ellipse indicates the location of oil-bearing reservoir. Black curve represents P-wave velocity provided by well log.

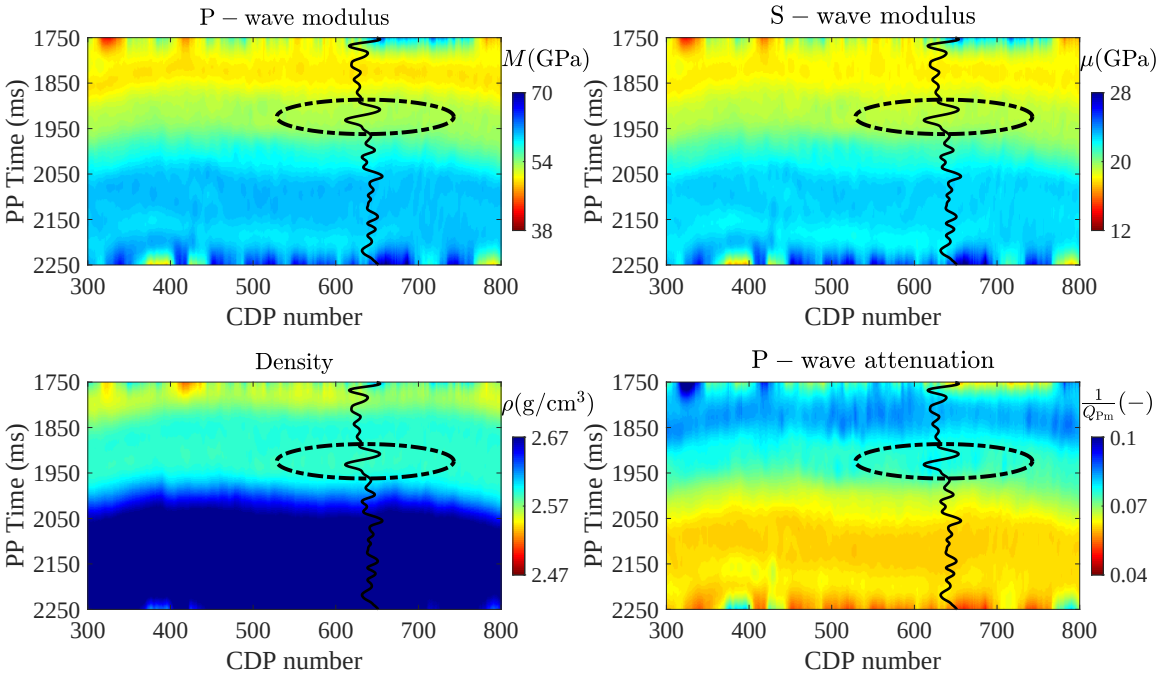

FIG. 12. Constructed initial models of P- and S-wave moduli, density and P-wave attenuation factor. Dashed ellipse indicates the location of oil-bearing reservoir. Black curve represents P-wave velocity provided by well log.

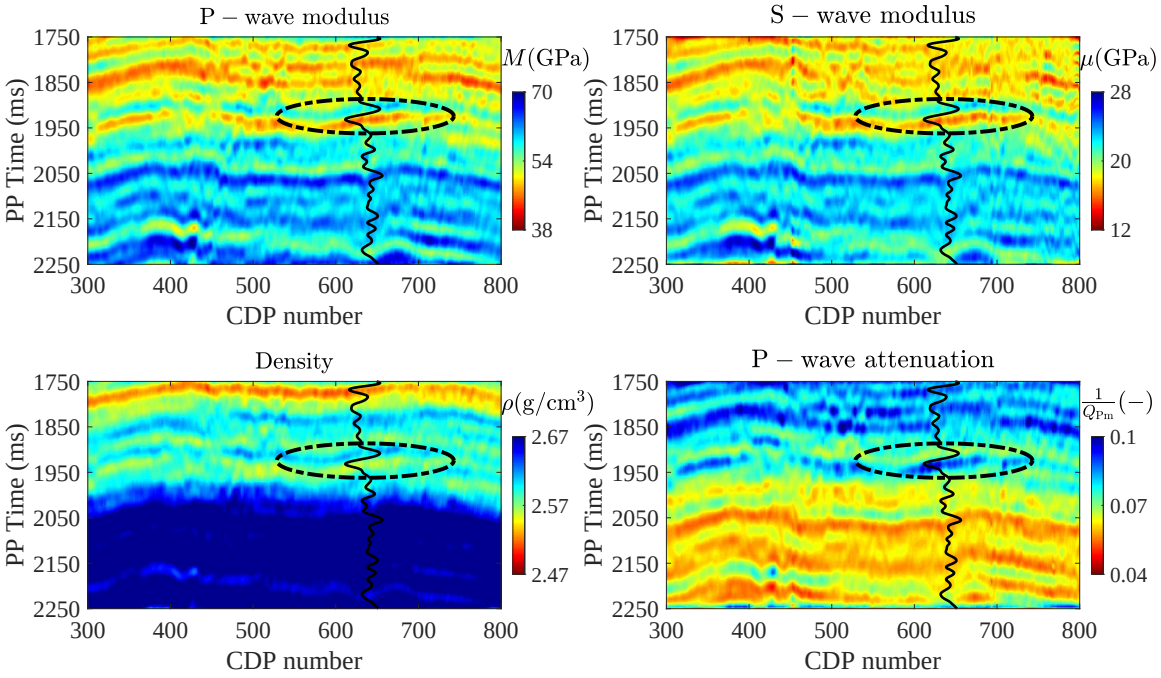

FIG. 13. Inversion results of P- and S-wave moduli, density and P-wave attenuation factor. Dashed ellipse indicates the location of oil-bearing reservoir. Black curve represents P-wave velocity provided by well log.

Council of Canada) through the grant CRDPJ 461179-13. This work was also funded in part thanks to the Canada First Research Excellence Fund, and the Mitacs Accelerate grant *Responsible Development of Unconventional Hydrocarbon Reserves*. The SINOPEC Key

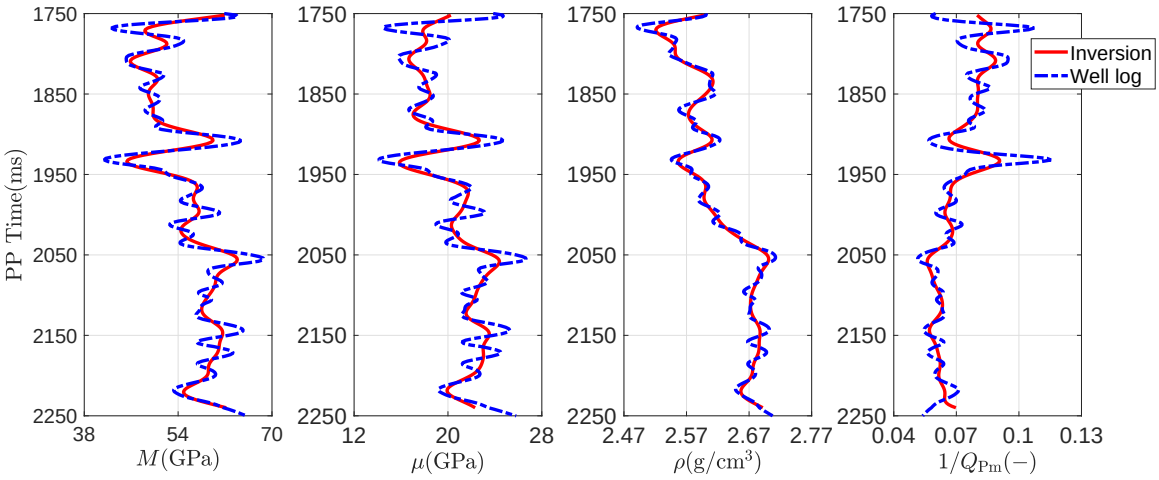

FIG. 14. Comparisons betwen inversion results and well log data of P- and S-wave moduli, density and P-wave attenuation factor. Dashed curves represent well log data, and solid curves represent inversion results.

Lab of Multi-Component Seismic Technology is thanked for providing the processed real data.

REFERENCES

Aki, K., and Richards, P. G., 2002, Quantitative seismology: University science books.

Berryman, J. G., 2007, Seismic waves in rocks with fluids and fractures: Geophysical Journal International, **171**, No. 2, 954–974.

Biot, M. A., 1956a, Theory of propagation of elastic waves in a fluid-saturated porous solid. I. Low-frequency range: The Journal of the acoustical Society of America, **28**, No. 2, 168–178.

Biot, M. A., 1956b, Theory of propagation of elastic waves in a fluid-saturated porous solid. II. Higher-frequency range: The Journal of the acoustical Society of america, **28**, No. 2, 179–191.

Bird, C., 2012, Amplitude-variation-with frequency (AVF) analysis of seismic data over anelastic targets: M.Sc. thesis, University of Calgary.

Brown, R. J., and Korringa, J., 1975, On the dependence of the elastic properties of a porous rock on the compressibility of the pore fluid: Geophysics, **40**, No. 4, 608–616.

Chen, H., Innanen, K. A., and Chen, T., 2018, Estimating P-and S-wave inverse quality factors from observed seismic data using an attenuative elastic impedance: Geophysics, **83**, No. 2, R173–R187.

Chen, H., Zhang, G., Chen, J., and Yin, X., 2014, Fracture filling fluids identification using azimuthally elastic impedance based on rock physics: Journal of Applied Geophysics, **110**, 98–105.

Dvorkin, J., Mavko, G., and Nur, A., 1995, Squirt flow in fully saturated rocks: Geophysics, **60**, No. 1, 97–107.

Dvorkin, J., Nolen-Hoeksema, R., and Nur, A., 1994, The squirt-flow mechanism: Macroscopic description: Geophysics, **59**, No. 3, 428–438.

Dvorkin, J., and Nur, A., 1993, Dynamic poroelasticity: A unified model with the squirt and the Biot mechanisms: Geophysics, **58**, No. 4, 524–533.

Dvorkin, J. P., and Mavko, G., 2006, Modeling attenuation in reservoir and nonreservoir rock: The Leading Edge, **25**, No. 2, 194–197.

Gassmann, F., 1951, Uber die elastizitat poroser medien: Vierteljahrsschrift der naturforschenden gesellschaft in zurich.

Geng, Y., Pan, W., and Innanen, K. A., 2018, Frequency-domain full-waveform inversion with non-linear descent directions: Geophysical Journal International, **213**, No. 2, 739–756.

Ikelle, L. T., and Amundsen, L., 2005, Introduction to petroleum seismology: Society of Exploration Geophysicists.

Innanen, K. A., 2011, Inversion of the seismic AVF/AVA signatures of highly attenuative targets: Geophysics, **76**, No. 1, R1–R14.

Köhn, D., 2011, Time domain 2D elastic full waveform tomography: Ph.D. thesis, University of Kiel.

Margrave, G. F., 2013, Q tools: Summary of CREWES software for Q modelling and analysis: the 25th Annual Report of the CREWES Project.

Mavko, G., and Jizba, D., 1991, Estimating grain-scale fluid effects on velocity dispersion in rocks: Geophysics, **56**, No. 12, 1940–1949.

Mavko, G., Mukerji, T., and Dvorkin, J., 2009, The rock physics handbook: Tools for seismic analysis of porous media: Cambridge university press.

Moradi, S., and Innanen, K. A., 2015, Scattering of homogeneous and inhomogeneous seismic waves in low-loss viscoelastic media: Geophysical Journal International, **202**, No. 3, 1722–1732.

Moradi, S., and Innanen, K. A., 2016, Viscoelastic amplitude variation with offset equations with account taken of jumps in attenuation angle: Geophysics, **81**, No. 3, N17–N29.

Morozov, I. B., 2011, Anelastic acoustic impedance and the correspondence principle: Geophysical Prospecting, **59**, No. 1, 24–34.

Pan, W., Innanen, K. A., Margrave, G. F., and Cao, D., 2015, Efficient pseudo-Gauss-Newton full-waveform inversion in the τ-p domain: Geophysics, **80**, No. 5, R225–R14.

Whitcombe, D. N., 2002, Elastic impedance normalization: Geophysics, **67**, No. 1, 60–62.